Pharmaceutical Research, Vol. 25, No. 11, November 2008 (© 2008)
DOI: 10.1007/s11095-008-9679-z

Research Paper

Miniaturized Rotating Disk Intrinsic Dissolution Rate Measurement: Effects of Buffer Capacity in Comparisons to Traditional Wood's Apparatus

Alex Avdeef[1,2] and Oksana Tsinman[1]

Received April 23, 2008; accepted June 27, 2008; published online July 22, 2008

Purpose. The objective was to investigate the feasibility of using a miniaturized disk intrinsic dissolution rate (IDR) apparatus to determine the Biopharmaceutics Classification System (BCS) solubility class, and to develop an approach where IDR measurements performed in media of different buffer capacity could be compared.
Methods. The disk IDR values of 14 model drugs were determined at 37°C in US Pharmacopeia buffers at pH 1.2, 4.5, and 6.8. As little as 5 mg of drug were compressed in a die, with surface area of 0.071 cm^2, with the die assembly rotated at 100 rpm in 10 mL media. Drug concentration was measured by an *in situ* fiber optic ultraviolet method. The solubilities and pK_as were determined, and used to simulate dissolution profiles with a convective-diffusion-with-chemical-reaction model.
Results. The disk IDR values spanned six orders of magnitude (0.00014 to 114 mg min^{-1} cm^{-2}). The comparison of the miniaturized disk IDR values to published results using traditional dissolution bath apparatus indicated r^2=0.99.
Conclusions. The results demonstrate that using 100-fold less drug does not sacrifice the quality of the measurement, and lends support to an earlier study Yu *et al.* (*Int. J. Pharm.* 270:221–227, 2004) that the disk IDR measurement may possibly serve as a surrogate for the BCS solubility classification.

KEY WORDS: Biopharmaceutics Classification System; buffer capacity; low solubility; rotating disk intrinsic dissolution rate; Wood's apparatus.

INTRODUCTION

The Biopharmaceutics Classification System (BCS) is a bioequivalence regulatory guideline (1), whose underlying premise is that *in vitro* measurement of dissolution, solubility, and permeability of solid-dosage oral drug products in aqueous media can predict their *in vivo* intestinal absorption performance (2). Solubility and permeability are used to define four classes in the BCS. A drug is considered highly soluble when its highest dose completely dissolves in 250 mL of aqueous media over the pH range 1.0 to 7.5. The rate and extent of intestinal absorption can be affected by a number of gastrointestinal tract variables: pH, ionic strength, buffer capacity, drug binding (proteins, bile salts, and lecithin), motility, and viscosity (3–5). For "practically insoluble" drugs that have high permeability (Class 2), dissolution and dose are critical factors for predicting the rate and extent of absorption (6).

During drug product development, investigative dissolution studies are often carried out with rotating disks of compacted powder of the active pharmaceutical ingredient (API) immersed in dissolution test media (Wood's method (7)). Disk intrinsic dissolution rates (IDR) are determined according to the equation: (8) $IDR = (dm/dt)_{max}/A$, where the units of IDR are milligram per minute per square centimeter, A is the area of the drug disk (square centimeter), m is the mass (milligram), t is the time (minute), and $(dm/dt)_{max}$ is the maximum slope in the dissolution curve, evaluated at the start of the dissolution process. Rotating disk IDR measurements have been used for many years to characterize solid drugs, including studies of dissolution-pH rate profiles in the presence of buffers, binding agents, and various excipients/delivery vehicles (9–21).

In the common modifications of the disk IDR method, about 150–700 mg of pure API are compressed in a punch and die to produce a pellet with an exposed surface area typically from 0.5 cm^2 (18) to 1.3 cm^2 (9). During the dissolution period, the exposed area of the disk is taken to be constant. Often, traditional six-vessel US Pharmacopeia (USP)-specified dissolution baths (22) are run at 37°C, accommodating volumes of 900 mL in each vessel. Usually, ultraviolet data are externally sampled at a particular wavelength to measure the concentration of the API as a function of time. Turbid solutions are traditionally filtered during external sampling in order to read the UV spectra reliably. Newer *in situ* fiber optic dip-probe methods require neither filtration nor external sampling of the dissolution media (23–29).

The feasibility of using IDR measurements to determine BCS solubility class membership was investigated by Yu *et al.* (18) The IDR values of 15 model drugs (six with low, nine with high solubility) were reported. Their proposed method consists of using about 500 mg of API compressed at 138 bar for 1 min into pellets of exposed surface area of 0.5 cm^2, with

Part 4 in the API-Sparing Dissolution Method series from *p*ION. Berger *et al.* (28) is Part 3 in the series.

[1] pION INC, 5 Constitution Way, Woburn, Massachusetts 01801, USA.
[2] To whom correspondence should be addressed. (e-mail: aavdeef@pion-inc.com)

measurements performed in 900 mL (or 225 mL) media at pH 1.2, 4.5, and 6.8 (USP buffers (22)), with disk rotation speed set at 100 rpm. The dissolution method was found to be a simple and convenient way to classify the solubility of drugs, using a proposed 0.1 mg min^{-1} cm^{-2} class boundary. However, it was stressed that more measurements were needed to test further the concept of using IDR as a substitute for solubility measurement in the BCS.

Although dissolution methods are applied traditionally in drug development, a case can be made for using such methods much earlier in drug discovery (26). As medicinal chemists scale up the synthesis of a particularly promising compound, it is not uncommon that the isolated solid is morphologically different in new batches. Dissolution measurements on small quantities of the compound can reveal polymorphic changes, and such compound-sparing small-volume dissolution screening can be very useful. However, such measurements appear to be rarely done in drug discovery.

In the earliest stages of development, when drug delivery is first explored and synthesis of promising compounds is scaled up further, there is often a shortage of the candidate material to do some of the desirable testing using traditional USP-type dissolution apparatus. API-sparing methods are essential (26, 28,30). Furthermore, these methods need to be media-sparing, especially when simulated intestinal fluid or human intestinal fluid are used. However, there appears to be a reluctance among some of the traditional dissolution practitioners—as noted in discussions at scientific meetings—to use very small dissolution media volumes, on concerns that the familiar (USP) "hydrodynamic and sink conditions" may not be maintained when media volumes are as low as 1–10 mL. If this concern can be alleviated, miniaturization of IDR methods (28,30) in early development can promote the increased, and much earlier, use of simulated gastrointestinal fluids to predict absorption properties of drug candidates (32).

The main objective of the study was to demonstrate that the miniaturized disk IDR apparatus and method can produce results of comparable reliability as those obtained by traditional Wood's apparatus methods, without the need for any scaling adjustments (30), and that the miniaturized apparatus can be potentially useful in BCS classification of solubility, applied at a much earlier time in the development cycle. We therefore investigated 14 compounds with the miniaturized disk IDR method, using as little as 5 mg to make compacted disks of 0.071 cm^2 exposed surface area, rotated in 10 mL of buffer media. Drug concentration was measured by an *in situ* fiber optic UV method. The measurements were conducted in pH 1.2, 4.5 and 6.8 buffer media, and both 50 and 200 mM buffer media were tested to illustrate the impact of buffer capacity (10,26) on measured IDR values. A new computational tool, (26,27) based on a generalized form of the convection-diffusion with chemical-reaction (CDR) models (9,10,13–15) was successfully used to theoretically simulate the IDR values obtained in buffers of different capacity.

MATERIALS AND METHODS

Drugs and Chemicals

Atenolol, carbamazepine, furosemide, glibenclamide, griseofulvin, haloperidol, hydrochlorothiazide, ketoprofen, labetolol hydrochloride, nadolol, naproxen, papaverine hydrochloride, piroxicam, and propranolol hydrochloride were purchased from Sigma-Aldrich (St. Louis, MO, USA). Standard buffers at pH 1.2 (85 mM HCl, 50 mM KCl), 4.5 (28 mM acetic acid, 22 mM sodium acetate, NaOH), and 6.8 (50 mM KH_2PO_4, NaOH) were made according to the USP Vol. 23 procedures (22). Four-fold concentrated (200 mM) versions of the pH 4.5 and 6.8 were also prepared.

pK_a Measurement

The Gemini Profiler (*p*ION) was used to determine the pK_a values of all the ionizable drugs studied here. For each compound, at least three replicate titrations were performed at 37±0.5°C in 1 mL of 0.15 M KCl medium. The titrated solutions were bathed with argon, to minimize the ingress of ambient carbon dioxide. The double-junction pH electrode was calibrated *in situ* (Avdeef-Bucher (35) 4-parameter procedure) under precisely the same conditions as the used for the pK_a determination, diminishing the need for traditional "blank" titrations (34). As typical procedures, acids were titrated from pH 12.2 to 1.8 with 0.5 M HCl, while bases were titrated from pH 1.8 to 12.2 with 0.5 M KOH. The methanol cosolvent procedure (34) was used for glibenclamide, where the apparent pK_a values at various ratios of cosolvent (13–30 wt.%) were extrapolated to zero-cosolvent to estimate the aqueous value. Some of the published dissolution studies cited here (9,10,13–17,21) used either high or highly variable ionic strength media. To address this, ketoprofen and atenolol were selected for an in-depth ionic strength dependence assessment, with each molecule titrated at six different ionic strengths (0.17 to 0.54 M KCl).

Determination of the pH at the Surface of the Solid ($pH_{x=0}$) and Interfacial Solubility Determination

The method of Serajuddin and Jarowski (11,12) was used to estimate the pH at the surface of dissolving solid. Enough solid to produce a saturated solution (8–400 mg) in 2 mL of buffers was weighed into vials, which were then sealed and allowed to stand at 37°C for 24 h, with occasional shaking. After that, the pH of the solutions containing excess solid was measured at 37°C with an electrode calibrated in a pre-warmed pH 7 buffer. These pH values were taken to be estimates of the pH at the surface of dissolving solid, as described elsewhere (11,12). Aliquots of the same saturated solutions were diluted in buffers and the concentrations of several of the drugs were determined by UV, using the μDISS Profiler*PLUS* spectrophotometric analyzer (*p*ION) and the method of multiple analyte additions (46). This measurement corresponds to "interfacial" solubility of the compound (at $pH_{x=0}$), a value which can be compared to that determined by the analysis of dissolution data.

Miniaturized Pellet Compression System

The Mini-IDR compression system (Heath Scientific, UK) was used to make miniaturized pellets. As little as 5 mg of the API powder is loaded into the cylindrical hole of a passivated stainless steel die and compressed (1 min at 120 bar) to a uniform, flat surface, with an exposed area of

0.071 cm^2 (Fig. 1a). The die can accommodate larger weights of API, if needed. Once compressed, the sample die is inserted into a cylindrical Teflon rotating disk carrier containing an embedded magnetic stir bar at its base (Fig. 1b). A black dot on the side of the cup (Fig. 1c) allows for independent rotation speed verification. The design of the die avoids complications due to edge effects (36) in the original Wood's design (7). The stirrer-die assembly is placed in a flat-bottomed glass vial ready for dissolution analysis, as shown in Fig. 1c.

In Situ Fiber Optic Dip-Probe UV Spectrophotometry and Miniaturized Bath Dissolution Apparatus

The μDISS Profiler*PLUS* instrument used in the dissolution measurements employs eight photodiode array (PDA) spectrophotometers, each with its own dedicated fiber optic dip probe, center-positioned in the vial holding the rotating disk carrier and 10 mL media (Fig. 1c). Stirring speed was set at 100±2 rpm and the temperature was set at 37±0.5°C. Some of the challenges of traditional dissolution testing methods which use external sampling of the test solutions (e.g., sampling errors due to filter clogging, mechanical sipper malfunction, sample contamination, adsorption of compound to tubing) were avoided by the use of the *in situ* fiber optic-dip probe UV apparatus, since the concentration measurements are performed directly in the dissolution media, with processed results plotted in "real time." Interference due to background turbidity is minimized by a spectral second derivative method (23–29). Spectral scans (200–720 nm) of all eight channels takes less than one second. The PDA baseline noise is ±0.0002 absorbance units.

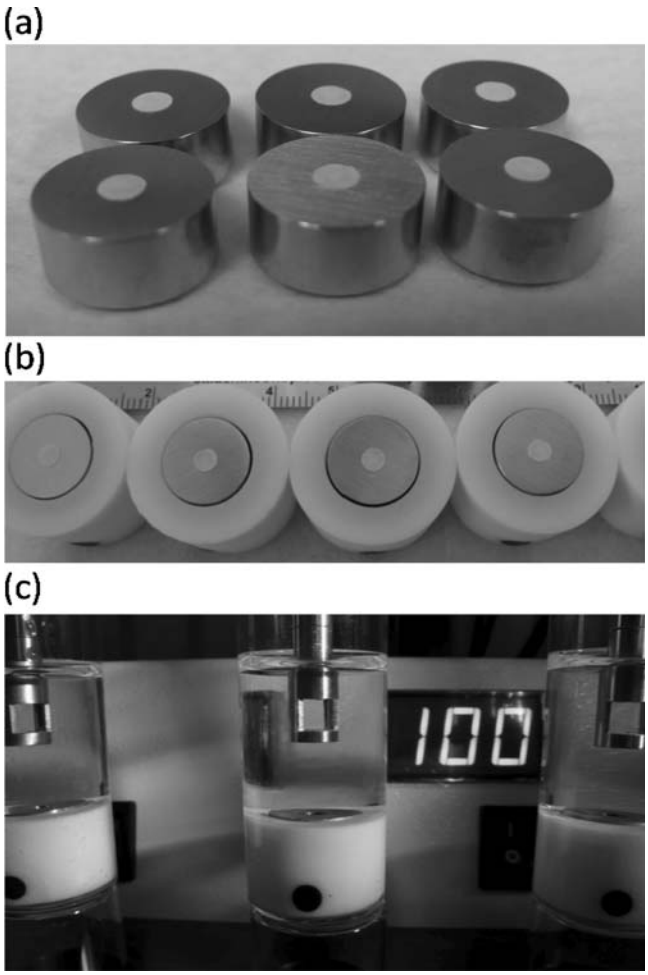

Fig. 1. Miniaturized rotating disk intrinsic dissolution rate sample holder: (**a**) stainless steel dies with compound pellets; (**b**) dies inserted into Teflon holders; (**c**) Teflon holder assembly in 10 mL media, with fiber optic probes inserted.

THEORETICAL SECTION

Thin-film Theory of Dissolution

IDR and solubility were determined by analyzing the dissolution profiles with an exponential expression, based on a simple solution to the Noyes–Whitney equation (8). However, to convert values of IDR measured at one buffer capacity to values at another buffer capacity, it was necessary to apply a much more complex theoretically calculation, based on a generalized form of the CDR model (9,10,13–15), as more recently described by Avdeef *et al.* (26) Other dissolution-related factors (such as micro-species distribution across the aqueous boundary layer (ABL), interfacial pH gradients, drug complexation with media components, interfacial effects of buffer capacity, and so on) can be addressed by the latter model.

Two-term Exponential Expression Used to Model Dissolution Data

The pseudo-steady-state rate of dissolution, dm/dt, and the solubility are related by the Noyes–Whitney (8) equation

$$dm/dt = AP_{\mathrm{ABL}}(S - C) \tag{1}$$

where P_{ABL} = permeability (centimeter per minute) across the aqueous boundary layer = D_{aq}/h_{ABL}, where D_{aq} = diffusivity in aqueous solution (square centimeter per minute), h_{ABL} = thickness (centimeter) of the ABL; C = concentration of solute (milligram per milliliter) dissolved in the bulk medium at a particular time, S = equilibrium solubility (milligram per milliliter) corresponding to the pH in the ABL in direct contact with the solid surface ($pH_{x=0}$, x = distance from surface). Initially, the dissolution rate is at its maximum and a sink state prevails ($C \approx 0$); the closer the system is to complete dissolution ($C \approx S$), the slower is the dissolution process.

From Fick's first law of diffusion (37–39), the one-dimensional steady-state flux, J (milligram per minute per square centimeter), is related to Eq. 1 as

$$\mathrm{J} = -D_{aq}(dC/dx) = (dm/dt)/A = P_{\mathrm{ABL}}(S - C) \tag{2}$$

IDR is the maximum flux, J_{max}, and can be defined, according to Eq. 2, as the maximum dissolution rate, DR_{max} ($t \approx 0$, effectively at a "sink state"), divided by A (Eq. 3a), or as the product of permeability and solubility (Eq. 3b).

$$\mathrm{IDR} = \mathrm{DR}_{\max}/A \tag{3a}$$

$$= P_{\mathrm{ABL}}S \tag{3b}$$

According to Eq. 3b, if a saturated solution forms at the end of dissolution, then IDR can be calculated *without knowledge of surface area* (provided that the surface area is constant). A solution to the Noyes–Whitney differential equation (Eq. 2) may be stated as (38)

$$C(t) = S \cdot \left(1 - e^{-\frac{A}{V} \cdot P_{\mathrm{ABL}} \cdot (t - t_o)}\right) \tag{4}$$

The three constants—S, A, and t_o ("lag" time preceding release of API, possibly due to "wettability" delay, etc.)—can be determined by weighted nonlinear least-squares refinement (40). In Eq. 4, the volume of the medium, V (milliliter), is known and P_{ABL} can be approximated, with the aid of the Levich equation (34, 37–39), as

$$P_{\mathrm{ABL}} = (1 + 0.028 \cdot (t_c - 25)) \cdot \frac{\left(10^{-4.15 - 0.448 \log \mathrm{MW}}\right)^{\frac{2}{3}}}{4.98\, \eta^{\frac{1}{6}} \cdot RPM^{-\frac{1}{2}}} \tag{5}$$

(in centimeter per second units), where t_c is the temperature (degree Celsius), η is the kinematic viscosity (0.00696 $\mathrm{cm^2\ s^{-1}}$ at 37°C, aqueous media), and MW is the molecular weight of the drug molecule.

The single-exponential function (Eq. 4) sometimes does not adequately describe the dissolution profile, which can appear "biphasic" in the release of the API. There are a number of possible underlying causes of the biphasic appearance. For example, two different solid forms of the API can participate in dissolution: (a) some loose powder, detaching from the pellet surface/edges, and (b) the solid in the pressed pellet itself. The loose powder is expected to be associated with a high surface area, but limited to a small quantity of material. The pellet has a small constant surface area, accounting for most of the compound quantity. The following two-component model function was used to address these biphasic process issues:

$$\begin{aligned} C(t) = {} & C_{\mathrm{powder}} \cdot \left(1 - e^{-\frac{A_{\mathrm{powder}}}{V} \cdot P_{\mathrm{ABL}} \cdot (t - t_o)}\right) \\ & + C_{\mathrm{pellet}} \cdot \left(1 - e^{-\frac{A_{\mathrm{pellet}}}{V} \cdot P_{\mathrm{ABL}} \cdot (t - t_o)}\right) \end{aligned} \tag{6}$$

In this definition, C_{powder} refers to the concentration in the solution at $t=\infty$ due to the contribution of the loose powder. The area associated with the powder is A_{powder}. The second term in Eq. 6 contains the contribution from the pellet. Nonlinear weighted regression analysis in the μDISS software was used to determine the five constants: C_{powder}, A_{powder}, C_{pellet}, A_{pellet}, t_o. The first derivative of Eq. 6 with respect to time, evaluated at the initial lag time, $t=t_o$, is the maximum dissolution rate, $\mathrm{DR_{max}}$ (in units of milligram per minute).

According to Eqs. 3a and 3b, for the rotating disk method, there are two operationally different ways to estimate the IDR value in a dissolution experiment, depending on whether the solid completely dissolves during compound release or whether a saturated solution forms in the end. For highly-soluble compounds, which fully dissolve at long dissolution times, IDR is defined by Eq. 3a, with $\mathrm{DR_{max}}$ derived as described in the preceding paragraph. On the other hand, for practically-insoluble compounds, which form a saturated solution at long dissolution times, the area need not be known, and IDR is defined by Eqs. 3b and 5. Furthermore, in the saturated solution ($t=\infty$), $\mathrm{pH_{medium}}$ becomes $\mathrm{pH}_{x=0}$ and $S = C_{\mathrm{powder}} + C_{\mathrm{pellet}}$.

Convective Diffusion with Chemical Reaction Rotating Disk Intrinsic Dissolution Rate of Ionizable Drugs

The overall dissolution rate of ionizable drugs depends on how quickly all of the chemically-reacting species (including the buffer components and the drug in its various charge states) diffuse through the ABL, which in turn depends on how strongly the drug interacts with the media components in the ABL, such as excipients, complexing agents, and especially to what extent pH gradients consequently develop in the ABL. This level of detail is beyond the scope of the preceding biphasic model (Eq. 6). To predict how buffer capacity affects the dissolution rate, a more complex model than that of Eq. 6 needs to be considered (9–16,26,27).

The thin ABL adjacent to the surface of the dissolving solid, separating the solid–liquid interface from the bulk medium, is the rate-limiting barrier in dissolution. When the solid is added to the dissolution medium, almost instantaneously (assuming "wettability" is not an issue), the concentration of the drug at the solid–liquid interface ($x=0$) becomes equal to its "surface" solubility, which may be different from the expected bulk-solution solubility. The reason for this is simply that the pH at the surface may not be the same as the pH of the bulk solution at the start of dissolution, and this can lead to buffer capacity dependence in IDR measurements (9–15). After a further short delay (typically <0.5 s (26)), the steady-state is established (dm/dt becomes constant near $x \approx 0$). At that time, the sink condition is still in effect (since the amount of drug dissolved in the bulk medium, $x > h_{\mathrm{ABL}}$, is vanishingly low), and the linear concentration gradient (at $x=0$) which initially drives the dissolution process (Fick's law) is equal to the solubility at $\mathrm{pH}_{x=0}$ divided by h_{ABL}. As more compound dissolves (>10% of the solubility value), the process becomes more complicated to analyze (due to non-sink conditions), but the concentration of the drug at the solid–liquid "surface" still remains equal to the solubility at $\mathrm{pH}_{x=0}$. Dissolution will continue until the concentration of the drug in the bulk medium becomes equal to the solubility (and the bulk medium pH equals to $\mathrm{pH}_{x=0}$), or until all the solid dissolves.

Equations in Convective Diffusion Mass Transport

The dissolved molecules move through the ABL, away from the solid surface, by the combined action of diffusion and the convective fluid flow generated by the action of the rotating disk. Simultaneously, some of the medium components will migrate towards the surface. The convective flow equations due to the rotation in a viscous fluid were originally solved by von Kármán in 1921, and later substantially refined by Cochran in 1934, as described in classic books by Levich (39), Cussler (38), and Schlichting and Gersten (37).

The partial differential equation describing the convective diffusion process, both before and after the onset of steady state, is stated as

$$\partial C(x,t)/\partial t = \partial(D(x) \cdot \partial C(x,t)/\partial x)/\partial x + |V(x)| \cdot \partial C(x,t)/\partial x \tag{7}$$

where $C(x,t)$ is the concentration of the reactant, at position x (distance from the surface of the rotating disk) and time, t. $D(x)$ is the diffusivity at position x (which indirectly has a time dependence), and $|V(x)|$ is the absolute value of the axial velocity of the convective fluid flow, at distance x from the rotating surface. Each different species in solution has its own form of Eq. 7. For example, for a diprotic weak acid (e.g., hydrochlorothiazide or furosemide), the different species are H_2A, HA^-, A^{2-}, H^+ and OH^- (in unbuffered solution). Normally, Eq. 7 needs to be solved for $C(x,t)$ of each of the species (the treatment of chemical reaction terms, not denoted in Eq. 7, is described below).

Vinograd–McBain Treatment of Diffusion of Electrolytes and of the Ions in Their Mixture

Electric fields, created in solutions containing ions migrating under concentration gradients, can act on each ion, to either retard or accelerate its diffusion velocity from the canonical value the ion would have (D*) in the absence of the gradients. If a solution contains a highly mobile ion, like H^+, and a more slowly diffusing ion, like the charged drug molecule, and there is an imposed concentration gradient, the faster ion has the innate tendency to diffuse ahead of the slower ion, which creates a charge separation. This in turn lowers the diffusivity of the fast ion and raises that of the slow one, so that very quickly both ions travel at the same steady-state velocity, in order to maintain spatial charge neutrality. Such changes in diffusivity inside the ABL need to be properly accounted for in the analysis of dissolution experiments, *particularly when the ionic strength of the solution is low*.

Vinograd and McBain (41) derived the expression for the diffusivity at position x in the ABL for a given ion, $D_j(x)$, as a fraction of the diffusivity that the ion would have in the absence of concentration gradients, D_j^* (position independent),

$$\frac{D_j(x)}{D_j^*} = 1 \mp \frac{|z_j| \cdot C_j(x,t)}{\left(\frac{dC_j(x,t)}{dx}\right)} \cdot \left\{ \frac{\sum_i \frac{z_i}{|z_i|} D_i^* \left(\frac{dC_i(x,t)}{dx}\right)}{\sum_i D_i^* |z_i| \, C_i(x,t)} \right\} \quad (8)$$

where the '–' sign in $\mp$ is used if the species j is a cation, and the '+' used if it is an anion. The summations are taken over all ions present in solution. The shifts in the diffusivity coefficients predicted by Eq. 8 are less dramatic when an appreciable amount of background salt, e.g., 0.5 M KCl, is added. For a weak acid example, the coupling between A^- and H^+ is relaxed by the K^+ and Cl^- ions from the "swamping" level of background electrolyte. Equation 8 is incorporated in the μDISS-X computer program developed to solve Eq. 7 (26).

Chemical Reaction During Convective Diffusion

Once an ionizable substance dissolves and begins to diffuse across the ABL, it may undergo chemical reactions, as noted above. Yet, Eq. 7 does not explicitly contain reaction terms. It was shown by Olander (42) that if the differential equations for each species, such as, e.g., Eq. 7 applied to H_2A, HA^-, A^{2-}, H^+, and OH^-, are combined to express *total* concentrations of weak acid drug, C_{tot}, all reaction terms cancel out, provided the reactions are reversible and fast compared to diffusion (42). It is simply not necessary to consider explicit chemical reaction rate constants. For example, the total partial differential expression for the diprotic weak acid (e.g., hydrochlorothiazide or furosemide) becomes

$$\begin{aligned} \partial C_{tot}/\partial t = {} & \partial(D_{H2A} \cdot \partial C_{H2A}/\partial x)/\partial x \\ & + \partial(D_{HA} \cdot \partial C_{HA}/\partial x)/\partial x \\ & + \partial(D_A \cdot \partial C_A/\partial x)/\partial x + |V(x)| \cdot \partial C_{tot}/\partial x \end{aligned} \quad (9)$$

Equation 9 can be solved for the total concentrations C_{tot}. With C_{tot} calculated, then the nonlinear computation of all reactant and associated species can proceed, provided all the relevant equilibrium constants are known. A general and robust numerical method to solve Eq. 9 has been described (26). A very fast analytical solution was also described (26). All CDR calculations in our present study were performed by μDISS-X.

RESULTS AND DISCUSSION

pK_a Determination

Ionization constants can be dependent on both ionic strength and temperature (34). Since reliable published pK_a values measured at 37°C and physiologically-relevant ionic strength were not available for most of the molecules studied here, the values were determined in the present study (Table I). Fig. 2 shows pK_a values of atenolol and ketoprofen, as a function of ionic strength. Atenolol shows a positive slope (+0.251 M^{-1}), whereas the Debye–Hückel theory predicts zero ionic-strength dependence (34). The published atenolol value in 0.15 M KCl at 25°C is 9.54 (34), compared to 9.19 at 37°C. Such temperature dependence (−0.029 deg^{-1}) is typical of weak bases (34). On the other hand, ketoprofen shows practically no temperature dependence (+0.003 deg^{-1}) between 25°C (3.98 (34)) and 37°C (4.02), which is also typical of many monoprotic carboxylic acids. Ketoprofen shows negative (but attenuated, compared to theory) ionic strength dependence (−0.147 M^{-1}).

In the case of furosemide, haloperidol, ketoprofen, and naproxen titrations, some precipitation was observed during the titration, but it was not necessary to resort to the traditional cosolvent method for these molecules, since the software in the Gemini Profiler allows for direct pK_a determination when there is some precipitation during a portion of the titration (33,34). So, it appears to be possible to use aqueous media, provided the intrinsic solubility of the molecule, $S_o \geq 2.5$ μg/mL (that of haloperidol (19)). Glibenclamide, with $S_o = 0.35$ μg/mL (44), is below this threshold, and the cosolvent method (34) was needed to determine its pK_a.

Since many low-soluble NSAIDs can self-aggregate to form micelles and micelle-like structures above a critical concentration (43), determination of their pK_a values from solubility-pH profiles can be unreliable (26,27,34,44,45). Possibly, the pK_a value of ketoprofen at 37°C reported as 4.76 (21) and 4.60 (43) are "apparent" values (45), that differ

Table I. Ionization Constants, Interfacial pH and Solubility of Ionizable Drugs

Compound	$pK_a \pm SD^a$	pK_a^a temp. dep. (deg^{-1})	Ionic str. (M)[b]	Buffer concn. (M)[c]	Buffer pH	Interfacial $pH_{x=0}$[d]	Wt (mg) drug added to 1 mL buffer	S (mg mL^{-1}) ± SD[d]
Atenolol	9.19±0.01	-0.029	0.15	0.2	4.5	9.24	110	–
				0.2	6.8	9.29	92	27±3
Furosemide	9.87±0.01	-0.063	0.20	0.2	4.5	4.47	–	–
	3.51±0.01	-0.001		0.2	6.8	6.47	52	7.9±0.4
Glibenclamide	5.88±0.05	+0.011	0.18	0.05	5.0	4.46		
				0.029	6.5	6.53		
Haloperidol	8.35±0.02	-0.020		0.05	4.5	4.94	11	
				0.05	6.8	6.83	4	
Hydrochloro thiazide	9.78±0.01	-0.014		0.2	4.5	4.5		
	8.53±0.01	-0.019		0.2	6.8	6.8		
Ketoprofen	4.02±0.01	+0.003	0.15	0.2	4.5	4.48	–	–
				0.2	6.8	6.08	61	11.2±0.1
				0.05	6.8	5.64	59	3.1±0.1
Labetolol.HCl	9.00±0.01	-0.035	0.20	0.05	1.2	1.01	12	6.4±0.2
	7.25±0.01	-0.019		0.05	4.5	4.57	40	21.8±0.1
				0.05	6.8	5.62	23	6.1±0.1
Nadolol	9.38±0.01	-0.026		0.2	4.5	8.97	130	–
				0.2	6.8	9.04	77	20±4
Naproxen	4.00±0.04	-0.015	0.19	0.2	4.5	4.47	–	–
				0.2	6.8	6.59	51	5.6±0.1
Papaverine.HCl	6.20±0.02	-0.016		0.05	6.8	6.43	4	
Piroxicam	5.34±0.02	+0.023	0.15	0.05	1.2	1.23		
				0.05	4.5	4.44		
				0.05	6.8	6.75		
Propranolol.HCl	9.17±0.02	-0.030	0.17	0.2	4.5	4.40	148	
				0.2	6.8	6.13	200	

All measurements at 37° C
[a] Determined by potentiometric titration (Gemini Profiler). Temperature dependence estimated from the difference between 37° C (this work) and 25° C (lit. (34)) pK_a values
[b] Total ionic strength (0.15 M KCl medium)
[c] pH 1.2: HCl/KCl; pH 4.5 and 5.0: acetate buffer; pH 6.5 and 6.8: phosphate buffer
[d] Solubility and pH measured after 24 h incubation

quite substantially from the true pK_a value of 4.02. Also, the McIlvaine buffer used for pH control (21), changes significantly in ionic strength over its working pH range (31), further challenging precise pK_a determination by the solubility-pH method.

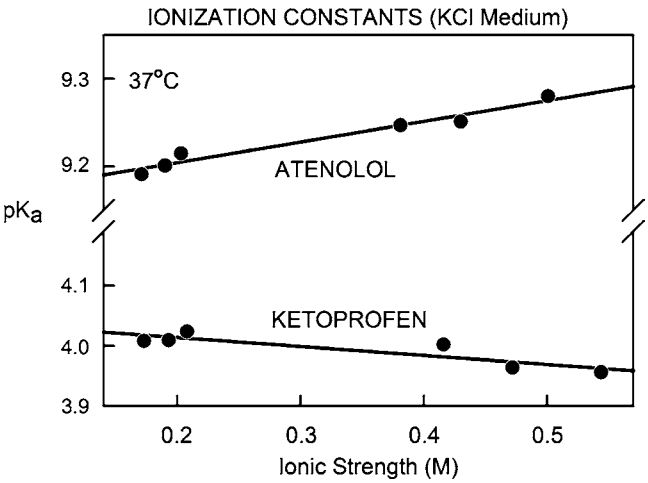

Fig. 2. Atenolol and ketoprofen pK_a values at 37°C, as a function of ionic strength.

Surface pH ($pH_{x=0}$) and Interfacial Solubility

Table I lists the measured pH and the concentrations of drug in saturated solutions for the ionizable set. In the thin-film model, the latter two quantities can be equated to the pH at the surface ($pH_{x=0}$) of a dissolving solid and the interfacial solubility which drives the dissolution process at that $pH_{x=0}$ (11,12). For example, atenolol (free base) indicates that neither the pH 4.5 (0.2 M acetate) nor the pH 6.8 (0.2 M phosphate) buffer has sufficient capacity to resist the pH-altering effect of the dissolving compound. At the start of dissolution, the bulk pH is either 4.5 or 6.8, but at the solid–liquid contact surface, $pH_{x=0}$ rapidly sets to 9.24 and 9.29, respectively. Given enough solid to form a saturated solution at the end of the dissolution process, the entire bulk medium adopts the pH that was originally at the solid-liquid interface. The less soluble and/or less ionized the molecule is, the smaller is the difference between bulk and interfacial pH. The higher the buffer capacity of the medium, the smaller is the difference between bulk and interfacial pH.

Dissolution Profiles

Two to six replicate dissolution experiments were performed for each compound. For each compound studied,

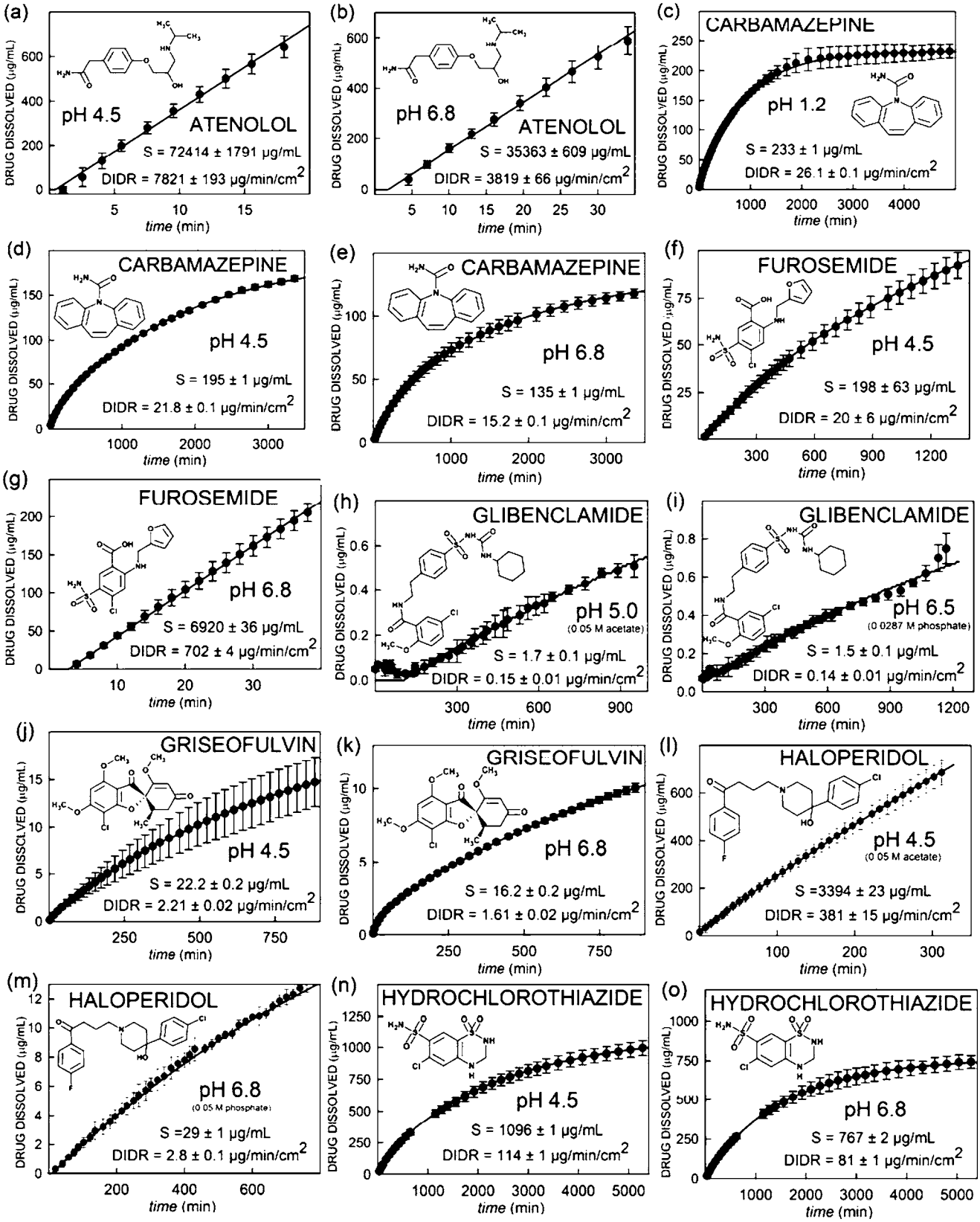

Fig. 3. a–zd Dissolution profiles. DIDR = disk IDR.

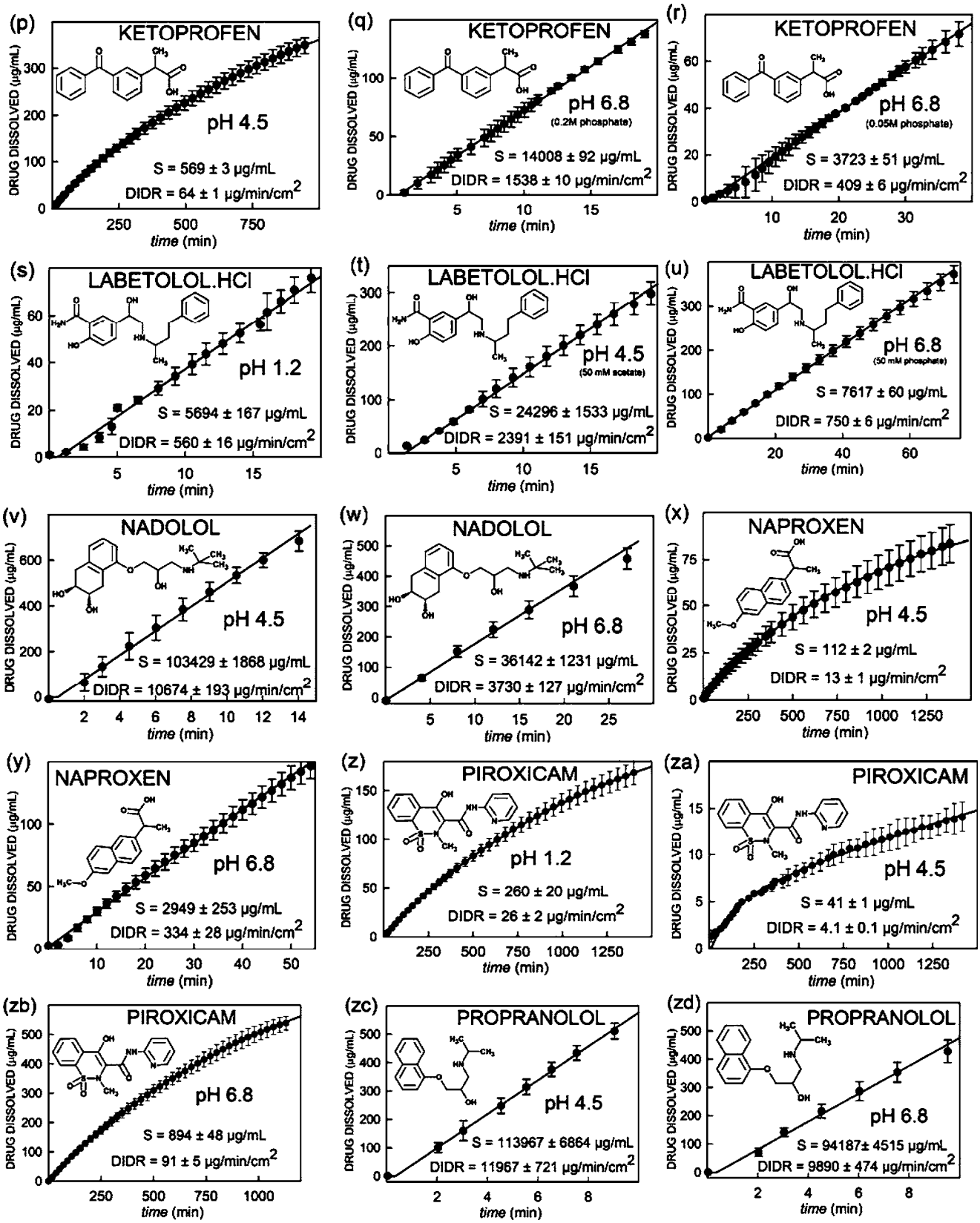

Fig. 3. (continued).

Table II. Biphasic Model Refinement Results

COMPOUND	MW	P_{ABL} (cm s^{-1})	Buffer pH	C_{powder} (mg mL^{-1})	SD	A_{powder} (cm^2)	SD	Cpellet (mg mL^{-1})	SD	Apellet (cm^2)	SD	t_0 (min)	SD	GOF	Number	No. curves
Atenolol	266.3	1.80E-03	4.5					72.4	1.8	0.075		0.6	0.2	0.3	9	6
			6.8					35.4	0.6	0.075		1.8	0.2	0.3	11	6
Carbamazepine	236.3	1.87E-03	1.2	0.0120	0.0004	2.82	0.28	0.221	0.001	0.152	0.001	-8.8	1.1	0.3	51	2
			4.5	0.0162	0.0002	1.24	0.03	0.178	0.001	0.075		1.4	0.5	0.3	35	3
			6.8	0.0262	0.0006	0.53	0.02	0.109	0.001	0.075		-2.1	0.6	0.2	42	3
Furosemide	330.8	1.69E-03	4.5	0.025	0.026	0.34	0.15	0.17	0.06	0.057	0.049	22.9	0.5	0.1	33	6
			6.8					6.92	0.04	0.129		2.9	0.1	0.2	18	6
Glibenclamide	494.0	1.50E-03	5.0					0.0017	0.0001	0.075		99.3	23.5	0.0	21	3
			6.5					0.0015	0.0001	0.075		-66.2	26.0	0.3	22	3
Griseofulvin	352.8	1.66E-03	4.5	0.0005	0.00001	7.19	0.39	0.0217	0.0002	0.182	0.002	-1.3	0.1	0.0	40	2
			6.8	0.0012	0.00002	5.78	0.29	0.0150	0.0002	0.154	0.003	-2.7	0.4	0.2	40	2
Haloperidol	375.9	1.63E-03	4.5	0.0217	0.0034	1.69	0.40	3.37	0.02	0.071		-5.5	0.4	0.0	34	6
			6.8	0.0037		0.17	0.02	0.025	0.0004	0.071		9.1	0.9	0.3	41	3
Hydrochlorothiazide	297.7	1.74E-03	4.5	0.091	0.003	0.66	0.02	1.005	0.003	0.062	0.001	1.3	0.2	0.1	33	3
			6.8	0.034	0.002	1.09	0.06	0.733	0.002	0.089	0.001	4.1	0.3	0.1	34	3
Ketoprofen	254.3	1.83E-03	4.5	0.016	0.001	1.82	0.09	0.553	0.002	0.131	0.001	1.9	0.1	0.0	40	6
			6.8					14.01	0.09	0.075		0.6	0.1	0.4	25	6
			6.8					3.72	0.05	0.071		0.0	0.3	0.4	24	2
labetolol.HCl	364.9	1.64E-03	1.2					5.69	0.17	0.071		0.6	0.1	1.1	18	3
			4.5					24.3	1.5	0.071		1.2	0.3	1.9	15	3
			6.8					7.62	0.06	0.071		-0.6	0.2	0.4	19	5
Nadolol	309.4	1.72E-03	4.5					103	2	0.075		0.5	0.1	0.3	8	5
			6.8					36	1	0.075		0.5	0.3	0.5	5	6
Naproxen	230.3	1.88E-03	4.5	0.0030	0.0003	4.01	0.65	0.109	0.002	0.126	0.005	-2.8	0.4	0.1	33	6
			6.8					3.0	0.3	0.126		-0.7	2.0	2.9	25	6
Papaverine.HCl	375.9	1.63E-03	6.8					0.03	0.01	5	3	0.1		3.9	14	4
(transient salt)								0.074	0.001	64		0.1	0.0	0.4	40	
Piroxicam	331.4	1.69E-03	1.2	0.0054	0.0052	1.21	0.94	0.25	0.02	0.108	0.018	2.7	1.0	0.3	37	3
			4.5	0.0046	0.0005	1.16	0.25	0.036	0.03	0.033	0.003	9.0	7.3	0.9	39	2
			6.8	0.0242	0.0364	0.66	0.47	0.87		0.119	0.019	-0.5	0.0	0.1	43	2
Propranolol.HCl	295.8	1.75E-03	4.5					114	7	0.075		0.3	0.3	0.9	7	6
			6.8					94	5	0.075		0.4	0.2	0.6	6	6

Fit of Eq. 6 to dissolution curves. If SD values are not indicated, the preceding quantity was not refined.
SD Standard deviation, *n* number of points selected in the refinement, *GOF* goodness-of-fit

the averaged replicate concentration measurements along with the standard deviations (SD) at various time points are displayed in Fig. 3. The solid curves in each frame of Fig. 3 represent fitting of the dissolution data to Eq. 6. Table II lists the refined parameters resulting from the analysis (the parameters without accompanying SD were treated as unrefined contributions in Eq. 6). Also listed are the ABL permeability values for each compound, calculated according to Eq. 5. Table III lists the disk IDR and the solubility (at $pH_{x=0}$) values calculated from these parameters, as described in the Theoretical Section. These solubility values (Table III) compare reasonably well to those directly measured (Table I).

About a third of the determinations summarized in Table III had predicted complete dissolution of the compound at the end of the dissolution period (%D=100). For these highly soluble compounds, Eq. 3a was used to assess disk IDR, with the measured surface area of the disk provided as a fixed parameter in Eq. 6. For the compounds that were able to establish saturated solutions by the end of the dissolution period (%D<80), all parameters in Eq. 6 (or Eq. 4) were optimized in several cases (cf., Table II).

The IDR experiments summarized in Table II encompassed several earlier designs of dies, which had slightly larger diameter holes. In the case of poorly-soluble compounds, it was possible to determine the surface area by Eq. 6 analysis, and compare it to expected values based on direct measurement, with good agreement (data not shown). Also, the earliest designs of dies had a chamfer in the cylindrical holes (following Wood's original design (7)). This design subsequently was rejected, since the surface area at the start of dissolution did not match the surface area at the end. Nevertheless, it was possible to calculate the effect by

Table III. Disk Intrinsic Dissolution Rate and Solubility

COMPOUND	Buffer pH	%D	Buffer concn.(M)	IDR (mg cm^{-2} min^{-1})	SD	S (mg mL^{-1})	SD	I (mM)	β (mM pH^{-1})
Atenolol	4.5	100	0.2	7.8	0.2	72	2	88	111
			0.05	5.3	calc	49	calc	22	27
	6.8	100	0.2	3.8	0.1	35	1	444	107
			0.05	2.1	calc	19	calc	97	29
Carbamazepine	1.2	35	0.1	0.026	0.000	0.23	0.001	100	230
	4.5	29	0.2	0.022	0.000	0.19	0.001	88	111
	6.8	20	0.2	0.015	0.000	0.14	0.001	444	107
Furosemide	4.5	39	0.2	0.020	0.006	0.20	0.06	88	111
	6.8	100	0.2	0.70	0.004	6.9	0.04	447	107
			0.05	0.43	calc	4.0	calc	97	29
Glibenclamide	5.0	0	0.05	0.00015	0.00001	0.0017	0.0001		
	6.5	0	0.0287	0.00014	0.00001	0.0015	0.0001		
Griseofulvin	4.5	3	0.2	0.0022	0.00002	0.022	0.0002	88	111
	6.8	2	0.2	0.0016	0.00002	0.016	0.0002	444	107
Haloperidol	4.5	100	0.05	0.38	0.01	3.4	0.02	88	111
	6.8	1	0.05	0.0028	0.00004	0.029	0.0004	97	29
Hydrochlorothiazide	4.5	37	0.2	0.114	0.0005	1.10	0.004	88	111
	6.8	26	0.2	0.080	0.0002	0.77	0.002	444	107
Ketoprofen	4.5	70	0.2	0.063	0.0003	0.57	0.003	88	111
	6.8	100	0.2	1.54	0.01	14.0	0.09	447	107
			0.05	0.54	calc	4.9	calc	97	29
	6.8	100	0.05	0.41	0.01	3.7	0.05	97	29
Labetolol.HCl	1.2	100	0.05	0.56	0.02	5.7	0.2	100	230
	4.5	100	0.05	2.39	0.15	24.3	1.5	88	111
	6.8	100	0.05	0.75	0.01	7.6	0.1	97	29
Nadolol	4.5	100	0.2	10.7	0.2	103	2	88	111
			0.05	7.9	calc	76	calc	22	27
	6.8	100	0.2	3.7	0.1	36	1	447	107
			0.05	2.1	calc	20	calc	97	29
Naproxen	4.5	19	0.2	0.013	0.0002	0.11	0.002	88	111
	6.8	100	0.2	0.33	0.03	3.0	0.3	447	107
			0.05	0.23	calc	2.0	calc	97	29
Papaverine.HCl	6.8	1	0.05	0.0026	0.0006	0.026	0.006	97	29
(transient salt)		4		0.0073	0.0001	0.074	0.001	97	29
Piroxicam	1.2	20	0.05	0.026	0.002	0.26	0.02	100	230
	4.5	3	0.05	0.0041	0.0001	0.041	0.0005	88	111
	6.8	67	0.05	0.091	0.005	0.89	0.05	97	29
Propranolol.HCl	4.5	100	0.2	12.0	0.7	114	7	88	111
			0.05	11.9	calc	114	calc	22	27
	6.8	100	0.2	9.9	0.7	94	5	447	107
			0.05	11.8	calc	113	calc	97	29

%D is the maximum percentage dissolved at end of experiment
SD Standard deviation, *I* ionic strength, *β* buffer capacity

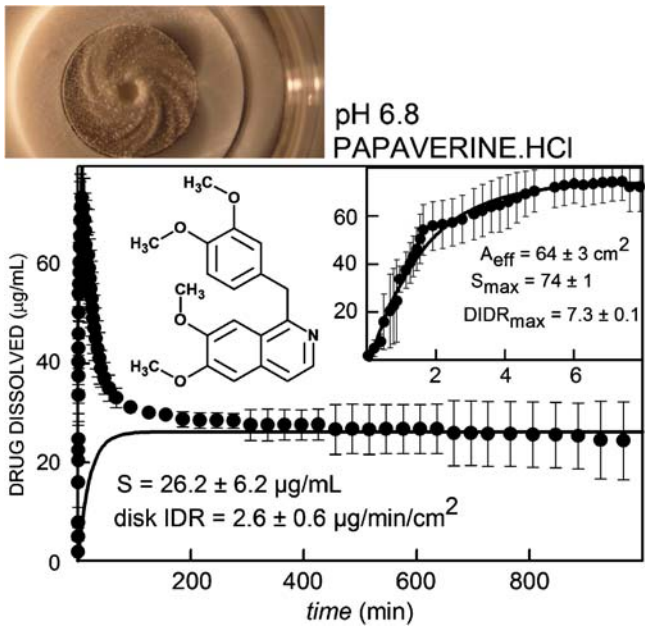

Fig. 4. Dissolution profile of papaverine hydrochloride at pH 6.8 (50 mM phosphate buffer). See text.

considering two surface areas in Eq. 6. In other cases, the two-area biphasic model improved the description of the dissolution profiles even though the dies were chamfer-free. Apparently in a few instances, a small amount of powder or solid bits detached from the die assembly of the compressed compound, and proceeded to dissolve more rapidly due to higher surface area compared to the compressed pellet (subsequently, we found that a gentle dusting of the surface of the disk before the start of dissolution decreases the "loose" powder contribution). In practice, Eq. 6 turned out to be a flexible and diagnostically useful data analysis tool.

The disk IDR (as well as solubility) values determined here spanned 6 orders of magnitude (0.00014 to 114 mg min^{-1} cm^{-2}). Although we could not find a published disk IDR value for glibenclamide, we selected the compound for the study to estimate the lower limit of reliable detection in the miniaturized dissolution apparatus. The disk IDR values for both pH 5 and 6.5 assays were about 0.00015 mg min^{-1} cm^{-2}, about 1,000 times below the proposed BCS high-to-low boundary classification value (18).

Papaverine Hydrochloride

Many hydrochloride salts of weak-base drugs dissolve relatively quickly but then re-precipitate in the neutral-pH media as free bases (5,11,12,19,20). Such was the trend shown by papaverine hydrochloride. The "rise-then-drop" pattern (Fig. 4) was distinctly different from dissolution profiles of the other molecules studied (Fig. 3). Of the six rotating disks tested with papaverine hydrochloride at pH 6.8 (50 mM buffer), two almost immediately and completely fragmented into a suspended flurry of powder. The other four disks showed a more controlled release of drug. Fig. 4 shows the averaged dissolution profile for the four disks that remained largely intact. Apparently, several processes were taking place at the beginning of dissolution (t<10 min): (a) rapid release of the charged form (BH^+) of the drug, (b) its subsequent neutralization (to the free base, B) in the phosphate buffer medium, (c) followed by precipitation of B onto the die and pellet surfaces of the rotating assembly, forming a "spiral dunes" flow pattern emanating out of the die orifice (Fig. 4). Very few detached particles were freely circulating. The maximum apparent solubility reached 0.074±0.001 mg mL^{-1} (Fig. 4, inset). The corresponding disk IDR maximized at 0.0073 mg min^{-1} cm^{-2}, indicated by the analysis of the dissolution profile for t<10 min using Eq. 4. The shape of the early dissolution curve is consistent with an apparent surface area of 64±3 cm^2 (presumably reflecting the effective surface area of the "dunes"). After 10 min, compound release rate started to decrease, presumably as the original hydrochloride salt form of the API rotating disk surface became covered with the free base solid. A similar phenomenon had been described

Table IV. Comparison of IDR Values (37°C, 100 rpm)

COMPOUND	Buffer pH	IDR [a] (mg min^{-1} cm^{-2})	Lit.	Ref.
Atenolol	4.5	5.31	3.74	18
	6.8	2.08	2.56	18
Carbamazepine	1.2	0.026	0.025	18
	4.5	0.022	0.024	18
	6.8	0.015	0.029	18
Furosemide	4.5	0.02	0.018	18
	6.8	0.43	0.502	18
Griseofulvin	4.5	0.0022	0.0019	18
	6.5	0.0016	0.0022	18
Haloperidol	4.5	0.381	0.246 [b]	19,20
	6.8	0.0028	0.002 [c]	19,20
Hydrochlorothiazide	4.5	0.114	0.124	18
	6.8	0.080	0.113	18
Ketoprofen	4.5	0.063	0.062	18
		0.066	0.059 [d]	21
	6.8	0.409	0.567	18
		0.540	0.567	18
		1.340	1.386 [e]	21
Labetolol.HCl	1.2	0.76 [h]	1.03	18
	4.5	2.39	2.88	18
	6.8	0.75	0.76	18
Nadolol	4.5	7.89	2.47	18
	6.8	2.11	1.44	18
Naproxen	4.5	0.013	0.012	18
	6.8	0.227	0.264	18
Piroxicam	1.2	0.026	0.022	18
	4.5	0.0041	0.0043	18
		0.0041	0.0040 [f]	17
	6.8	0.091	0.088	18
		0.091	0.092 [g]	17
Propranolol.HCl	4.5	11.9	13.3	18
	6.8	11.8	14.6	18

[a] This work. Underlined values were determined at buffer capacities, β (cf. Table III), different from those reported in the literature, and then adjusted by μDISS-X to match the reported buffer capacities
[b] Unbuffered solution; reported value at $pH_{x=0}$ 4.76 (19)
[c] Unbuffered solution; reported value at $pH_{x=0}$ 7.00 (19)
[d] pH 4.6: 103 mM phosphate, 49 mM citrate, β=43 mM pH^{-1}
[e] pH 6.8: 155 mM phosphate, 31 mM citrate, β=99 mM pH^{-1}
[f] Nonlinearly interpolated between pH 4 and 5 (17)
[g] Nolinearly interpolated between pH 6 and 7 (17)
[h] Doubly-underlined value transformed (μDISS-X) from USP pH 1.2 buffer formulation used here to 0.1 M HCl buffer used in (18).

for phenazopyridine hydrochloride (12). The concentration leveled off to a constant value of 0.026 mg mL^{-1} after about 10 h. The solid curve drawn in the main part of Fig. 4 represents a plausible dissolution curve, had the original pellet been made entirely of the free base, spread over a surface area of no less than 5 cm^2 (as drawn). Since the solution is evidently saturated at the end of the dissolution period, Eqs. 3b and 5 were used to determine the corresponding disk IDR value of 0.0026±0.0006 mg min^{-1} cm^{-2}. It was not necessary to include the surface area in the IDR calculation.

Labetolol Hydrochloride and Piroxicam—Reactions with Untreated Stainless Steel

Labetolol and piroxicam can react with stainless steel, especially in low-pH solutions where pH adjustment is effected by HCl, by forming red and orange iron complexes (putative). It is especially important to freshly passivate the stainless steel dies before use with drugs that may form metal complexes with iron. In the present study, the solutions and pellet surfaces remained colorless in all dissolution measurements with labetolol and piroxicam (slightly yellowish solution seen with piroxicam at the end of the dissolution period is not due to metal-complex formation (17)). The labetolol hydrochloride IDR values determined at pH 4.5 and 6.8 agree reasonably well with those reported in the literature (18), but a notable difference was found between the pH 1.2 IDR values (cf., Tables III and IV). The literature study (18) used 0.1 M HCl buffer for the pH 1.2 media. The USP formulation for the pH 1.2 buffer is slightly different, in that 0.05 M KCl is used, in addition to 0.085 M HCl. We applied μDISS-X transformation (using pK_a values from Table I and $K_{sp} = 2.39 \times 10^{-3} M^2$ from best-fit regression) to match the literature condition, and obtained an improved match (double-underlined entry in Table IV). Piroxicam appears to react with *untreated* stainless steel dies to a lesser extent than labetolol. The piroxicam IDR values determined here agree very well with those reported in the literature (17,18; Table IV).

Micro-speciation Analysis of Dissolution Profiles

To investigate the ABL micro-speciation contributions to dissolution of ionizable drugs by the CDR analysis (26), it is necessary to know the precise pK_a values of the API and all buffer components (37°C, appropriate ionic strength), and the intrinsic solubility, S_o (and the solubility product, K_{sp}, in the case of propranolol, naproxen, labetolol, and furosemide, since salt precipitation was indicated in the analysis of the dissolution data). The buffer pK_a values, interpolated to the correct temperature and ionic strength, were obtained from the buffer database in the Gemini Profiler (rev 3.0) software. The values of S_o (and/or K_{sp}, where needed) were estimated by regression analysis, based on minimization of the residuals between the measured IDR values (Table III) and those simulated by the μDISS-X software.

Fig. 5 shows two types of CDR speciation plots (26) for ketoprofen and atenolol, to illustrate the typical speciation complexity associated with an acid and a base API, depicted at the time point when steady state is reached (under sink condition). The horizontal scale represents the distance from the solid surface, in units of the ABL thickness, x/h_{ABL}.

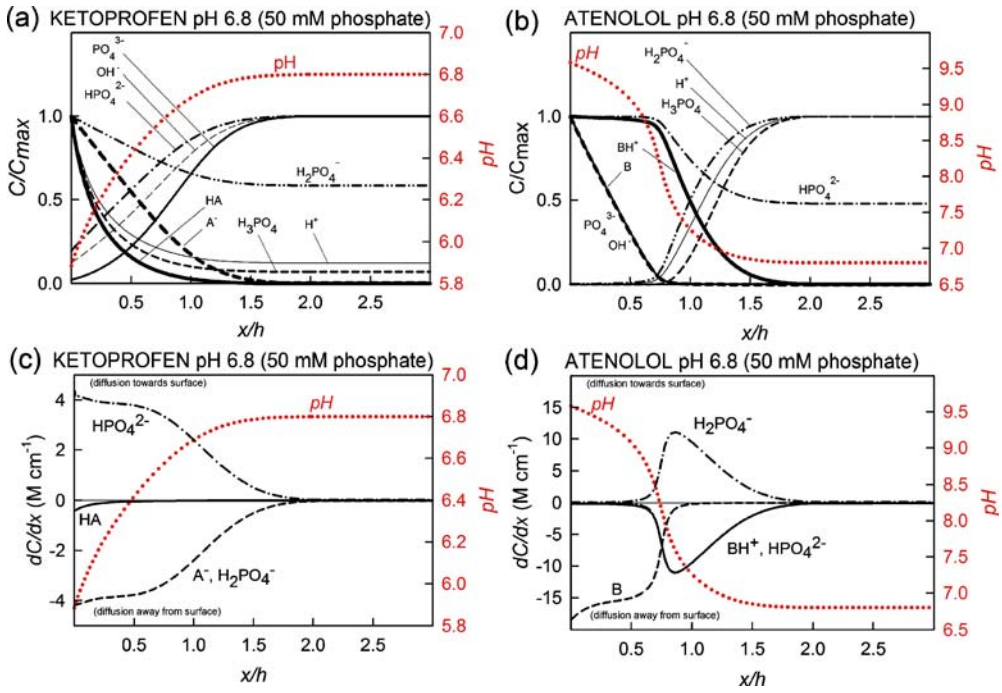

Fig. 5. Two types of simulated CDR speciation plots for ketoprofen (**a**, **c**) and atenolol (**b**, **d**) at pH 6.8 (50 mM phosphate buffer), as a function of the distance from the surface of the dissolving solid, in units of the thickness of the unstirred water layer: (**a**, **b**) relative concentrations of all species in the ABL; (**c**, **d**) concentration gradients, dC/dx, of all the micro-species in the ABL. The largest gradients are at the solid–liquid surface ($x=0$). The calculations correspond to time (t~0.4 s (26)) when the steady-state is first established, during which sink condition still holds.

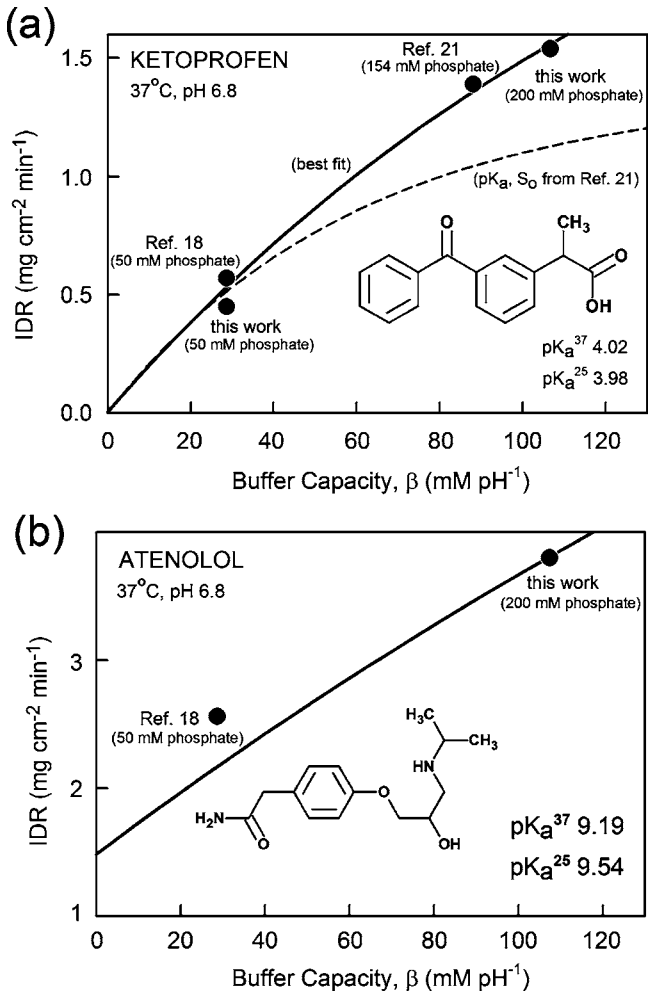

Fig. 6. Disk intrinsic dissolution rate plotted as a function of the buffer capacity, for ketoprofen (**a**) and (**b**) atenolol. The *points* are measured values; the *solid curves* are calculated by the CDR procedure (Eq. 9, see text). The *dashed curve* in (**a**) was calculated with pK_a and intrinsic solubility constants reported in the literature (21).

The top two frames in Fig. 5 display the relative concentrations of all the species in the solid-liquid boundary layer. These types of plots were first used by Mooney and Stella in their pioneering studies of dissolution (9,10).

Fig. 5c and d show the CDR-derived concentration gradients, dC/dx, of all the micro-species in the ABL. The largest gradients are at the solid–liquid surface ($x=0$). For ketoprofen, the dissolution flux primarily consists of the ketoprofen anion and the $H_2PO_4^-$ species co-migrating from the surface (negative concentration gradients) with an equal velocity. To maintain charge balance, the HPO_4^{2-} species migrates from the bulk solution to the surface (positive gradients). The concerted motion of the three species maintains local charge neutrality (cf., Eq. 8; 26). In the bulk pH 6.8 medium, the uncharged ketoprofen contributes minimally to transport (Fig. 5c). The case of atenolol (Fig. 5d) is more complex, in that neutralization takes place inside the ABL, in a zone called the "reaction plane" (9,10, 13–15,26). Up to about x/h_{ABL} of 0.75, uncharged atenolol migrates out of the solid surface. On reaching the reaction plane, atenolol becomes ionized. Past the reaction plane, cationic atenolol co-migrates outwardly with HPO_4^{2-}, while $H_2PO_4^-$ moves in the opposite direction (into the reaction plane), maintaining charge neutrality.

Reconciliation of IDR Values Determined at the Same Bulk pH but Different Buffer Capacity

Fig. 6a shows four ketoprofen IDR values, all determined at pH 6.8, but in different buffer capacity media. Our result and that of Yu *et al.* (18) in 50 mM phosphate buffer (29 mM pH^{-1} buffer capacity) are in the lower portion of the figure. The result reported by Sheng *et al.* (21) in McIlvaine buffer (pH 6.8; 0.48 M ionic strength), converted to milligram per minute per square centimeter units (Table IV), has the buffer capacity of 88 mM pH^{-1}, due mainly to the 154 mM phosphate in the buffer formulation. The highest IDR value corresponds to our result in 200 mM phosphate, at 107 mM pH^{-1} buffer capacity. To calculate the solid curves in the figure, we selected the intrinsic solubility as a regression parameter, and at 0.2 M buffer concentration, minimized the difference between the calculated and the measured IDR values. With the refined intrinsic solubility, we then calculated the whole curve for the range of buffer concentrations, using the CDR Eq. 9. That is, the solid curve in Fig. 6a was the result of fitting our 200 mM data point, by determining the best-fit intrinsic solubility, $S_o = 3.48 \times 10^{-4}$M , using the experimentally-determined pK_a 4.02 (Table I). When the apparent pK_a value and intrinsic solubility reported by Sheng *et al.* (21) were used for the CDR calculation, the fit was generally poor, as indicated by the dashed line. The solid

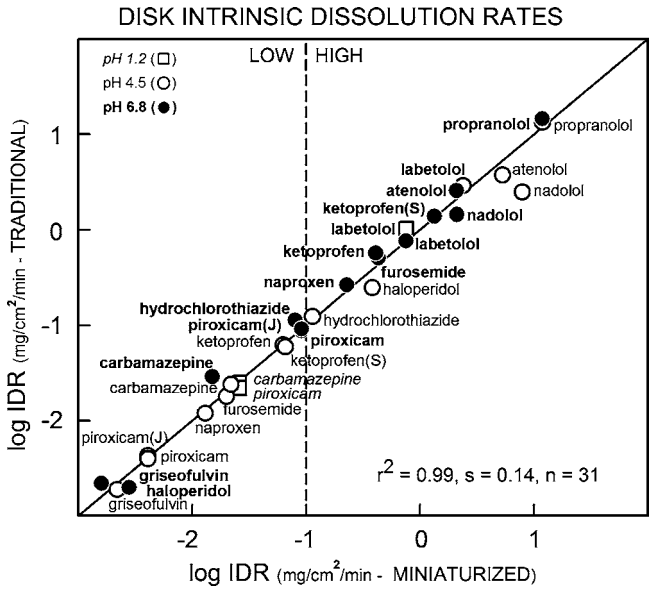

Fig. 7. Log–log correlation diagram, comparing published disk IDR values determined by traditional apparatus *vs.* values determined in this study, using miniaturized apparatus. Values determined in 200 mM buffer were CDR-transformed to match the buffer capacities of literature values. The compound names appended with (*J*) and (*S*) refer to (17) and (21), respectively. See text.

curve suggests that when a measurement is done in 200 mM phosphate buffer, it is possible to predict reasonably well the expected results in 154 or in 50 mM buffer, using the CDR calculation.

Figure 6b shows a similar IDR analysis for atenolol. For our 200 mM phosphate buffer determination (high point in the curve), the best-fit intrinsic solubility constant and the experimentally measured pK_a, produced the resultant IDR curve. The difference between the calculated atenolol IDR value at 29 mM pH^{-1} buffer capacity and the value reported by Yu *et al.* (18) is plotted in Fig. 7. All other compound IDRs that we measured at 200 mM were similarly transformed, to match the buffer capacity of the results reported in the literature.

Correlation of Miniaturized IDR Data to that Reported in the Literature Based on Traditional IDR Method

Table IV compares the literature IDR results cited here, based on traditional Wood's apparatus, to the results of the miniaturized IDR system. The underlined values in Table IV are the results determined in 200 mM buffer systems (cf., Table III), and CDR-transformed to the 50 mM level. Such transformations can be generally useful, because there is a range in buffer capacity of the media used in pharmaceutical assays today. For example, the buffer capacity in fasted/fed-state simulated intestinal fluids, FaSSIF/FeSSIF (3–6), differs from that of the traditional USP buffers (22). Other examples of common buffer media include phosphate-free Good's buffers for biological applications (31). To be able to adapt the traditional IDR methodology to encompass the variety of bio-mimetic buffer environments is a challenge that can be overcome, as our study suggests. Fig. 7 is the resultant correlation log–log plot, based on the values in Table IV. A very high correlation was achieved in the study, with r^2=0.99.

IDR as a Surrogate for Solubility in the BCS

The thick dotted lines in Fig. 5 simulations are the pH profiles in the ABL, with the pH scale indicated by the right axis. The μDISS-X calculated pH at the surface ($pH_{x=0}$) of the ketoprofen solid is below 6, even though the bulk pH is 6.8. In the case of atenolol, $pH_{x=0}$ is about 9.5, while the bulk pH is 6.8. Since the solubility term in the Noyes–Whitney expression (Eq. 1) refers to $pH_{x=0}$, not bulk pH, it can be misleading to associate the determined solubility—and thus the IDR—to the nominal pH of the buffer (Table III). In traditional investigative dissolution studies, apparently, $pH_{x=0}$ is often not measured at the end of the dissolution experiment. Table I shows that the buffer pH and $pH_{x=0}$ can be vastly different at the start of dissolution. Note (cf., Table III) that for ketoprofen at pH 6.8, the solubility determined from dissolution (Eq. 6 analysis) in 200 mM buffer is 14 mg mL^{-1}, but in 50 mM buffer the solubility value is 3.7 mg mL^{-1}—that is, for the same "buffer pH," the solubility can be substantially different. *If IDR is to be recommended as a useful surrogate for solubility classification in the BCS guideline, the relationship between the surface pH and the buffer pH needs to be reconciled, e.g., at least by direct measurement of pH in demonstrably saturated solutions at equilibrium.*

Conclusion

Our principal objective was to determine how well the miniaturized IDR apparatus and method correlates to published high-quality IDR data based on the traditional Wood's apparatus. An ancillary object was to determine if IDR data collected in a medium with a particular buffer capacity could be "corrected" to match the IDR results based in media with another buffer capacity. Our study suggests that both objectives were met. By demonstrating that the quantity of API used in traditional rotating disk apparatus could be reduced by a 100-fold without sacrificing the quality of the measurement, we are confident that (a) the concerns that the hydrodynamic and sink conditions will be affected by the miniaturizing of the rotating disk method may be alleviated, and that (b) the opportunity to consider investigative dissolution studies earlier in drug development is possible, in projects where API is not available in substantial amount.

REFERENCES

1. Guidance for Industry. *Waiver of in vivo bioavailability and bioequivalence studies for immediate release solid oral dosage forms based on a Biopharmaceutics Classification System*. FDA, Washington, D.C., 2000, August.
2. G. L. Amidon, H. Lennernäs, V. P. Shah, and J. R. Crison. A theoretical basis for a biopharmaceutic drug classification: the correlation of *in vitro* drug product dissolution and *in vivo* bioavailability. *Pharm. Res.* **12**:413–420 (1995), doi:10.1023/A:1016212804288.
3. J. B. Dressman, R. R. Berardi, T. L. Dermentzoglou, S. P. Russell, J. L. Schmaltz, J. L. Barnett, and K. M. Jarvenpaa. Upper gastrointestinal (GI) pH in young healthy men and women. *Pharm. Res.* **7**:756–761 (1990), doi:10.1023/A:1015827908309.
4. S. D. Mithani, V. Bakatselou, C. N. TenHoor, and J. B. Dressman. Estimation of the increase in solubility of drugs as a function of bile salt concentration. *Pharm. Res.* **13**:163–167 (1996), doi:10.1023/A:1016062224568.
5. E. S. Kostewicz, M. Wunderlich, U. Brauns, R. Becker, T. Bock, and J. B. Dressman. Predicting the precipitation of poorly soluble weak bases upon entry in the small intestine. *J. Pharm. Pharmacol.* **56**:43–51 (2004), doi:10.1211/0022357022511.
6. J. B. Dressman, G. L. Amidon, C. Reppas, and V. P. Shah. Dissolution testing as a prognostic tool for oral drug absorption: immediate release dosage forms. *Pharm. Res.* **15**:11–22 (1998), doi:10.1023/A:1011984216775.
7. J. H. Wood, J. E. Syarto, and H. Letterman. Improved holder for disk intrinsic dissolution rate studies. *J. Pharm. Sci.* **54**:1068 (1965), doi:10.1002/jps.2600540730.
8. A. S. Noyes, and W. R. Whitney. The rate of solution of solid substances in their own solutions. *J. Amer. Chem. Soc.* **19**:930–934 (1897), doi:10.1021/ja02086a003.
9. K. G. Mooney, M. A. Mintun, K. J. Himmelstein, and V. J. Stella. Dissolution kinetics of carboxylic acids I: effect of pH under unbuffered conditions. *J. Pharm. Sci.* **70**:13–22 (1981), doi:10.1002/jps.2600700103.
10. K. G. Mooney, M. A. Mintun, K. J. Himmelstein, and V. J. Stella. Dissolution kinetics of carboxylic acids II: effects of buffers. *J. Pharm. Sci.* **70**:22–32 (1981), doi:10.1002/jps.2600700104.
11. A. T. M. Serajuddin, and C. I. Jarowski. pH-solubility profile of papaverine hydrochloride and its relationship to the dissolution rate of sustained-release pellets. *J. Pharm. Sci.* **73**:1203–1208 (1984), doi:10.1002/jps.2600730905.
12. A. T. M. Serajuddin, and C. I. Jarowski. Effect of diffusion layer pH and solubility on the dissolution rate of pharmaceutical bases and their hydrochloride salts I: phenazopyridine. *J. Pharm. Sci.* **74**:142–147 (1985), doi:10.1002/jps.2600740208.

13. D. P. McNamara, and G. L. Amidon. Dissolution of acidic and basic compounds from the rotating disk: influence of convective diffusion and reaction. *J. Pharm. Sci.* **75**:858–868 (1986), doi:10.1002/jps.2600750907.
14. D. P. McNamara, and G. L. Amidon. Reaction plane approach for estimating the effects of buffers on the dissolution rate of acidic drugs. *J. Pharm. Sci.* **77**:511–517 (1988), doi:10.1002/jps.2600770610.
15. M. Z. Southard, D. W. Green, V. J. Stella, and K. J. Himmelstein. Dissolution of ionizable drugs into unbuffered solution: a comprehensive model for mass transport and reaction in the rotating disk geometry. *Pharm. Res*. **9**:58–69 (1992), doi:10.1023/A:1018979727118.
16. D. P. McNamara, M. L. Vieira, and J. R. Crison. Dissolution of pharmaceuticals in simple and complex systems. In G. L. Amidon, P. I. Lee, and E. M. Topp (eds.), *Transport Processes in Pharmaceutical Systems*, Marcel Dekker, New York, 2000, pp. 109–146.
17. J. Jinno, D. M. Oh, J. R. Crison, and G. L. Amidon. Dissolution of ionizable water-insoluble drugs: the combined effect of pH and surfactant. *J. Pharm. Sci.* **89**:268–274 (2000), doi:10.1002/(SICI)1520-6017(200002)89:2<268::AID-JPS14>3.0.CO;2-F.
18. L. X. Yu, A. S. Carlin, G. L. Amidon, and A. S. Hussain. Feasibility studies of utilizing disk intrinsic dissolution rate to classify drugs. *Int. J. Pharm.* **270**:221–227 (2004), doi:10.1016/j.ijpharm.2003.10.016.
19. S. Li, S. M. Wong, S. Sethia, H. Almoazen, Y. M. Joshi, and A. T. M. Serajuddin. Investigation of solubility of a free base and two different salt forms as a function of pH. *Pharm. Res*. **4**:628–635 (2005), doi:10.1007/s11095-005-2504-z.
20. S. Li, P. Doyle, S. Metz, A. E. Royce, and A. T. M. Serajuddin. Effect of chloride ion on dissolution of different salt forms of haloperidol, a model basic drug. *J. Pharm. Sci*. **94**:2224–2231 (2005), doi:10.1002/jps.20440.
21. J. J. Sheng, N. A. Kasim, R. Chandrasekharan, and G. L. Amidon. Solubilization and dissolution of insoluble weak acid, ketoprofen: effect of pH combined with surfactant. *Eur. J. Pharm. Sci*. **29**:306–314 (2006), doi:10.1016/j.ejps.2006.06.006.
22. The United States Pharmacopeial Convention. *United States Pharmacopeia* (*USP 23*). The United States Pharmacopeial Convention, Rockville, 1995.
23. K. Bynum, K. Roinestad, A. Kassis, J. Pocreva, L. Gehriein, F. Cheng, and P. Palermo. Analytical performance of a fiber optic dissolution system. *Dissol. Tech.* **8**:13–22 (2001).
24. V. A. Gray. Dissolution testing using fiber optics—a regulatory perspective. *Amer. Pharm. Rev.* **6**:26–30 (2003).
25. C. J. Toher, P. E. Nielsen, A. S. Foreman, and A. Avdeef. *In situ* fiber optic dissolution monitoring of vitamin B12 solid dosage formulation. *Dissolut. Tech*. **Nov**:20–25 (2003).
26. A. Avdeef, D. Voloboy, and A. Foreman. Dissolution and solubility. In B. Testa, and H. van de Waterbeemd (eds.), *Comprehensive Medicinal Chemistry II,* Vol. 5 ADME-TOX Approaches, Elsevier, Oxford, 2006, pp. 399–423.
27. A. Avdeef. Solubility of sparingly-soluble drugs. In J. Dressman, and C. Reppas (Eds.) The Importance of Drug Solubility). *Adv. Drug Deliv. Rev*. **59**:568–590 (2007), special issue, doi:10.1016/j.addr.2007.05.008.
28. C. M. Berger, O. Tsinman, D. Voloboy, D. Lipp, S. Stones, and A. Avdeef. Miniaturized intrinsic dissolution rate (Mini-IDR™) measurement of griseofulvin and carbamazepine. *Dissolut. Tech.* **14**:39–41 (2007).
29. V. Bijlani, D. Yuonaye, S. Katpally, B. N. Chukwumezie, and M. C. Adeyeye. Monitoring ibuprofen release from multi-particulates: *in situ* fiber-optic technique *versus* the HPLC method. *AAPS Pharm.Sci.Tech. 8*, (2007) Article 52 (http://www.aapspharmscitech.org). doi:10.1208/pt0803052
30. A. M. Persson, K. Baumann, L. -O. Sundelöf, W. Lindberg, A. Sokolowski, and C. Pettersson. Design and characterization of a new miniaturized rotating disk equipment for *in vitro* dissolution rate studies. *J. Pharm. Sci.* 2008, in press. Published online Nov 2007.
31. D. D. Perrin, and B. Dempsey. *Buffers for pH and Metal Ion Control*. Chapman and Hall, London, 1974.
32. H. Wei, and R. Löbenberg. Biorelevant dissolution media as a predictive tool for glyburide a class II drug. *Eur. J. Pharm. Sci.* **26**:45–52 (2006), doi:10.1016/j.ejps.2006.05.004.
33. S. Bendels, O. Tsinman, B. Wagner, D. Lipp, I. Parrilla, M. Kansy, and A. Avdeef. PAMPA-excipient classification gradient maps. *Pharm. Res.* **23**:2525–2535 (2006), doi:10.1007/s11095-006-9137-8.
34. A. Avdeef. *Absorption and Drug Development.* Wiley, Hoboken, 2003.
35. A. Avdeef, and J. J. Bucher. Accurate measurements of the concentration of hydrogen ions with a glass electrode: calibrations using the Prideaux and other universal buffer solutions and a computer-controlled automatic titrator. *Anal. Chem.* **50**:2137–2142 (1978), doi:10.1021/ac50036a045.
36. R. N. Jashnani, P. R. Byron, and R. N. Dalby. Validation of an improved Wood's rotating disk dissolution apparatus. *J. Pharm. Sci.* **82**:670–671 (1993), doi:10.1002/jps.2600820626.
37. H. Schlichting, and K. Gersten. *Boundary Layer Theory*, 8th ed. Springer, Berlin, 2000.
38. E. L. Cussler. *Diffusion–Mass Transfer in Fluid Systems*, 2nd ed. Cambridge Univ. Press, Cambridge, 1997, pp. 70–72.
39. V. G. Levich. *Physiochemical Hydrodynamics*. Prentice-Hall, Englewood Cliffs, 1962, pp. 39–72.
40. P. Bevington, and D. K. Robinson. *Data Reduction and Error Analysis for the Physical Sciences*, 3rd ed. McGraw-Hill, New York, 2002.
41. J. R. Vinograd, and J. W. McBain. Diffusion of electrolytes and of the ions in their mixture. *J. Amer. Chem. Soc.* **63**:2008–2015 (1941), doi:10.1021/ja01852a063.
42. D. R. Olander. Simultaneous mass transfer and equilibrium chemical reaction. *A.I.Ch.E. J.* **6**:233–239 (1960).
43. A. Fini, G. Fazio, and G. Feroci. Solubility and solubilization properties of non-steroidal antiinflammatory drugs. *Int. J. Pharm.* **126**:95–102 (1995), doi:10.1016/0378-5173(95)04102-8.
44. A. Avdeef, S. Bendels, O. Tsinman, and M. Kansy. Solubility–excipient classification gradient maps. *Pharm. Res.* **24**:530–545 (2007), doi:10.1007/s11095-006-9169-0.
45. A. Avdeef. Drug ionization and physicochemical profiling. In R. Mannhold (ed.), *Drug Properties: Measurement and Computation*, Wiley, Hoboken, 2007, pp. 55–83.
46. A. Avdeef, and J. Comer. A versatile potentiometric analyzer, part two: multiple known addition and Gran titration techniques. *Amer. Lab.* **19**:116–124 (1987).